The Astrophysical Journal Supplement Series, 175:543–556, 2008 April

ELECTRON-IMPACT IONIZATION OF Be-LIKE C III, N IV, AND O V

M. Fogle, E. M. Bahati, M. E. Bannister, and C. R. Vane
Physics Division, Oak Ridge National Laboratory, Oak Ridge, TN 38731-6372; bannisterme@ornl.gov

S. D. Loch and M. S. Pindzola
Department of Physics, Auburn University, Auburn, AL 36849

C. P. Ballance
Department of Physics, Rollins College, Winter Park, FL 32789

R. D. Thomas and V. Zhaunerchyk
Department of Physics, Stockholm University, S106 91 Stockholm, Sweden

and

P. Bryans, W. Mitthumsiri, and D. W. Savin
Columbia Astrophysics Laboratory, Columbia University, New York, NY 10027
Received 2007 August 13; accepted 2007 November 2

ABSTRACT

We present recent measurements of absolute electron-impact ionization cross sections for Be-like C III, N IV, and O V forming Li-like C IV, N V, and O VI. The measurements were taken using the crossed-beams apparatus at Oak Ridge National Laboratory. A gas cell beam attenuation method was used to independently measure the metastable fractions present in the ion beams. The measured ionization cross sections were compared with calculations using the *R*-matrix with pseudostates and distorted-wave theoretical methods. Best agreement is found with the *R*-matrix with pseudostates cross sections results that account for the metastable fractions inferred from the gas attenuation measurements. We present a set of recommended rate coefficients for electron-impact single ionization from the ground state and metastable term of each ion.

Subject headings: atomic data — atomic processes — methods: laboratory

1. INTRODUCTION

Electron ionized plasmas are ubiquitous throughout the cosmos. Such collisionally ionized gas is found, for example, in stellar coronae, supernova remnants (SNRs), the interstellar medium, galaxies, and clusters of galaxies. Spectral observations of these sources, in combination with theoretical models, are used to determine their physical properties. From this, one can infer electron and ion temperatures, densities, emission measure distributions, ionization history, and ion and elemental abundances. However, our ability to infer these properties rests in part on an accurate model for the fractional abundance of the different ionization stages of the various elements in the observed plasmas (i.e., the ionization balance).

Many of these collisionally ionized sources are not in local thermodynamic equilibrium. Determining the ionization balance of the gas thus requires knowledge of the rate coefficients for all possible ionization and recombination processes. These data are needed both for plasmas in collisional ionization equilibrium (CIE) conditions such as in stars and galaxies or nonequilibrium ionization (NEI) conditions such as in SNRs.

Of particular importance for CIE and NEI calculations are reliable electron impact ionization (EII) rate coefficients. For cosmically abundant elements with atomic numbers $Z \leq 28$, astrophysicists have long used the recommended EII data from Arnaud and her collaborators (Arnaud & Rothenflug 1985; Arnaud & Raymond 1992). Another important source of recommended EII data, used primarily by the plasma physics community, is the Belfast group (Bell et al. 1983; Lennon et al. 1988). These two groups both used essentially the same theoretical and experimental data. Surprisingly, however, the derived recommended rate coefficients sometimes differ by a factor of 2–3 at temperatures relevant for astrophysical plasmas (Kato et al. 1991; Savin 2005; Bryans et al. 2006). It has been clear for quite a while now that a re-evaluation of the EII database is necessary.

Recently Dere (2007) has reviewed the available EII theoretical and experimental results for all elements with $Z \leq 30$. Using the available literature and carrying out new distorted wave calculations using the Flexible Atomic Code (FAC; Gu 2002), Dere has developed a complete set of ground state EII data for all ions of all elements with $Z \leq 30$. However, a major theme running through his paper is the lack of reliable EII experimental results due to metastable contamination in the ion beams used. This severely hampers the reliability of using EII experimental results to benchmark EII theory.

To address the need for reliable EII rate coefficients for astrophysics, and predating the work of Dere (2007) we have initiated a systematic experimental and theoretical study of EII. Here we present our results for EII of Be-like ions of C, N, and O forming Li-like ions. Our experimental work benefits greatly from our ability to accurately and independently determine the metastable ion fraction of our ion beams.

Here we also pay particularly close attention to the plasma temperatures where Be-like C, N, and O are predicted to form in CIE and NEI. For CIE the fractional abundance of these ions are predicted to be greater than 1% in the ranges of 2–15, 5–24, and 10–40 eV, respectively (Bryans et al. 2006). In NEI such as occurs in SNR shocks, these Be-like ions form immediately after the shock and before substantial equilibration of the shock has occurred (Laming et al. 1996). At this point the electron temperature is ~300 eV (Ghavamian et al. 2007).

The rest of this paper is organized as follows: § 2 discusses the previously published theoretical and experimental work for EII

of Be-like C, N, and O. Section 3 describes the experimental setup and metastable fraction determination. We describe the theoretical methods in § 4. Our experimental and theoretical results for C^{2+}, N^{3+}, and O^{4+} are presented in § 5. This section also includes our recommended rate coefficients. In § 6 we present our conclusions.

2. PREVIOUS WORK

2.1. *Theoretical*

There have been a range of theoretical EII calculations for C^{2+}, N^{3+}, and O^{4+}. Salop (1976) carried out binary encounter calculations. Moores (1978) calculated results in the no-exchange Coulomb-Born approximation for C^{2+} and N^{3+}. Jakubowicz & Moores (1981) performed distorted-wave and Coulomb-Born with exchange calculations. Younger (1981b) carried out distorted-wave calculations with exchange. Ganas & Green (1981) used the atomic independent particle approximation for O^{4+}. McCarthy & Stelbovics (1983) presented continuum optical results for N^{3+}. McGuire (1997) performed plane-wave Born approximation calculations for C^{2+}. Loch et al. (2003) carried out distorted-wave calculations for O^{4+}.

There are several commonly used sources for EII rate coefficients of Be-like C, N, and O ions. Bell et al. (1983) use the Coulomb-Born calculations of Jakubowicz & Moores (1981) with a small contribution for inner shell ionization added. Bell et al. (1983) note that the results of distorted-wave calculations of Younger (1981b) are in good agreement with theirs. The Be-like EII rate coefficients given by Arnaud & Rothenflug (1985) are based on the Younger (1981b) distorted-wave calculations but neglect any contributions from excitation-autoionization (EA). Mazzotta et al. (1998) reference the work of Arnaud & Rothenflug (1985) in their review of ionization balance in optically thin plasmas. The work of Voronov (1997) uses a form of the Bell et al. (1983) data in which a correction for apparent metastable fractions of then available experimental data has been applied. This hierarchical referencing of different data sources shows a strong dependence on the distorted-wave calculations of Younger (1981b) with the work of Bell et al. (1983) being the exception.

Our group has extensive experience in EII calculations using perturbative distorted-wave methods and has published results for all ions in the Fe (Pindzola et al. 1987), Ni (Pindzola et al. 1991), Kr (Loch et al. 2002), and W (Loch et al. 2005b) isonuclear sequences. Recently, we have carried out EII calculations for the Be (Colgan et al. 2003) isonuclear sequence using the nonperturbative time-dependent close-coupling (TDCC) and *R*-matrix with pseudostates (RMPS) methods. We have also used nonperturbative methods to calculate EII of Li^+ (Berengut et al. 2007; Pindzola et al. 2000), O^+ (Loch et al. 2003), C^{2+} (Loch et al. 2005a), and various H-like atomic ions (Griffin et al. 2005). Our work has led to the observation that even for cases in which perturbative distorted-wave theory may do well for ground state ionization, it performs less well for ionization of metastable levels (Loch et al. 2005a) and excited levels (Griffin et al. 2005).

2.2. *Experimental*

Be-like ions present a particularly challenging case to study EII experimentally, due to the significant metastable $2s2p\ ^3P_{0,1,2}$ fractions expected in the ion population. All three *J*-levels have relatively long lifetimes. In $^{12}C^{2+}$, $^{14}N^{3+}$, and $^{16,18}O^{4+}$, which have zero nuclear spin, the $J = 0$ levels can decay only to the ground $^1S_0$ level via the emission of two or more photons (Schmieder 1973). The lifetimes are predicted to be $\approx 2 \times 10^{10}$, 5×10^9, and 1.5×10^9 s, respectively (Laughlin 1980). For the $J = 1$ levels, the measured lifetimes are ≈10, 2, and 0.045 ms for C^{2+}, N^{3+}, and O^{4+}, respectively (Doerfert et al. 1997; Träbert et al. 2002). Lastly, for the $J = 2$ levels, the theoretical lifetimes are ≈190, 91, and 30 ms for C^{2+}, N^{3+}, and O^{4+}, respectively (Glass 1982). Thus, for typical EII experiments, one would expect that any metastable ions extracted from an ion source would remain unchanged during the approximately one microsecond flight time to the interaction region. As an aside, we note that these long lifetimes also bring into question the validity of the assumption in plasma modeling that ground state rate coefficients are sufficient for determining an accurate ionization balance.

EII of C^{2+} has been studied experimentally by Hamdan et al. (1978), Woodruff et al. (1978), and Falk et al. (1983). Experimental results for EII of N^{3+} have been published by Falk et al. (1983) and for O^{4+} by Falk et al. (1983) and Loch et al. (2003). Significant metastable fractions were present in the Be-like ions used. Woodruff et al. (1978) noted the presence of metastables in their ion beam but did not estimate the fraction. Falk et al. (1983) estimated metastable fractions of 0.65 and 0.90 in a set of low and high metastable fraction experiments they undertook using a Penning ion gauge source. Recently the work of Loch et al. (2005a) inferred a 0.60 metastable fraction in C^{2+} measurements made at the CRYRING storage ring. This matched an estimate of the metastable fraction from a dielectronic recombination experiment taken in conjunction with the EII data using the same source conditions and storage parameters (Fogle et al. 2005).

The measurements of Hamdan et al. (1978), Woodruff et al. (1978), and Falk et al. (1983) were found to differ significantly from distorted-wave calculations when metastable fractions of ∼0.50 were assumed. The recent CRYRING storage ring measurements are in good agreement with these older measurements (Loch et al. 2005a). All of these experiments were considered to have similar ion beam metastable fractions, i.e., ∼0.50. Loch et al. (2005a) found that the distorted-wave calculations for ionization from the $2s^2$ ground and $2s2p$ excited configurations were overestimating the ionization cross sections, and that when nonperturbative calculations were used, including *R*-matrix with pseudostates, converged close-coupling, and time-dependent close-coupling, good agreement with all experimental measurements was found. But independently quantifying the metastable fractions remains an issue of concern.

Brazuk et al. (1984) studied the metastable Be-like fractions produced by an electron cyclotron resonance (ECR) ion source for a range of ions using a spectroscopic technique that utilizes excitation processes due to core-conserving electron capture. They found the fraction of metastable ions to be 0.56 ± 0.11 for C^{2+}, 0.52 ± 0.08 for N^{3+}, and 0.42 ± 0.06 for O^{4+}. The results tend to decrease with increasing *Z*. In addition, Brazuk et al. (1984) found that the metastable fractions are independent of the ion source discharge parameters. The metastable output, therefore, seems to be inherent to the basic source design and plasma characteristics. Despite these results, no systematic study of ion beam metastable fractions has been undertaken for different ion sources.

Arnaud & Rothenflug (1985) have pointed out the difficulty of extracting a ground state cross section due to the contribution of metastable ions. Reliably and independently determining the metastable fraction in the ion beam has been the main source of uncertainty in interpreting experimental EII cross section measurements used to benchmark various theories. In the past, metastable fractions have often been determined by a fit of experimental EII data below the ground state threshold by using a mixture of metastable and ground state theoretical cross sections (Bliek et al. 1997). This defeats the aim of using experiment to benchmark theory. One

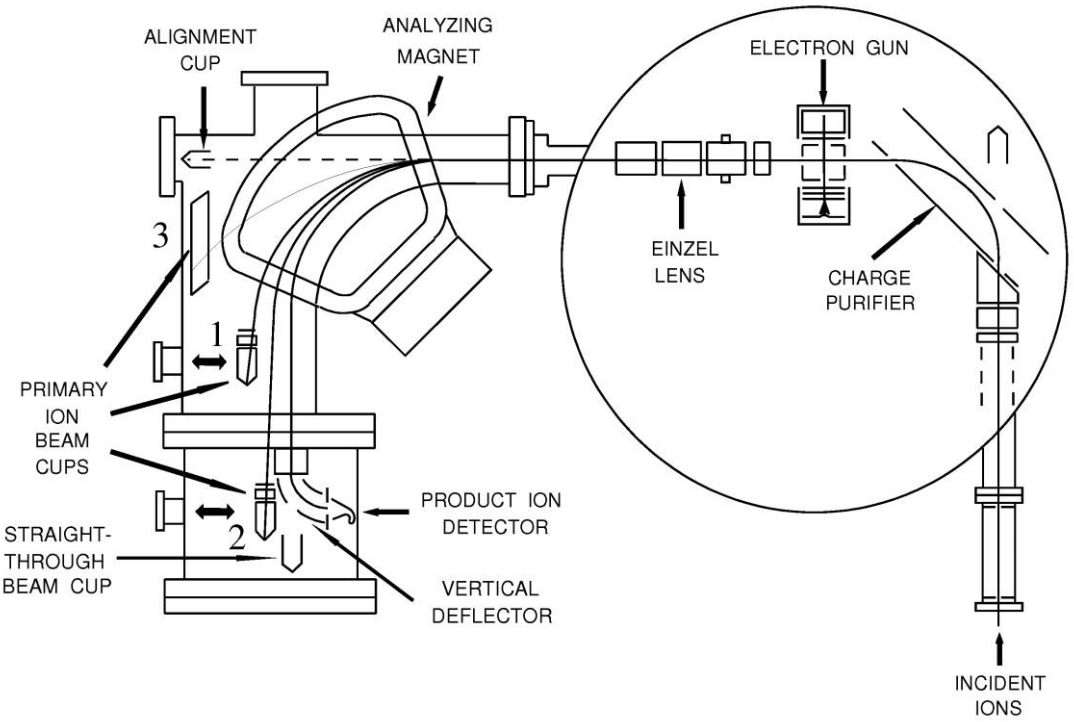

FIG. 1.—Schematic of the ORNL electron-ion crossed beams apparatus. See text for details.

goal of our work here is to determine the metastable fraction of our ion beams without having to rely on theoretical EII or DR work.

3. EXPERIMENT

3.1. *Absolute Electron-Impact Ionization Cross Sections*

Detailed discussions have been published describing our experimental approach using the crossed electron and ion beams technique for studying electron-impact ionization (Gregory et al. 1983; Bannister 1996). Here we briefly summarize our experimental methods and apparatus. Be-like ions were produced by a 10 GHz CAPRICE-type ECR ion source (Geller 1996; Meyer 2001). $^{12}CO_2$, $^{14}N_2$, and $^{18}O_2$ were used as the working gases in the ECR source in producing C^{2+}, N^{3+}, and O^{4+}, respectively. The working gas $^{18}O_2$ was chosen in order to avoid ion beam impurities from $^{12}C^{3+}$, which has the same mass-to-charge ratio as $^{16}O^{4+}$. However, tests with $^{16}O_2$ as the working gas resulted in little carbon contamination in the ion beam, as confirmed by a mass spectrum of the ion beam extracted from the source. The ion source was operated with microwave powers of 15–50 W and working gas pressures of approximately 10^{-6} Torr. Charged particles produced by the ECR source were extracted at energies of $10q$ keV, where q is the ion charge, and momentum analyzed by a 90° bending magnet.

Figure 1 gives a schematic overview of the ORNL crossed beams apparatus. Incident ions are charge-state purified by a 90° electrostatic parallel plate analyzer in order to remove ions that might have undergone charge exchange processes with residual gas atoms during their flight from the ion source to the crossed beams apparatus. The purified ions then enter the interaction region, where they are orthogonally crossed with a magnetically confined electron beam produced by an indirectly heated cathode. The electron energy is set by biasing the electron gun acceleration elements located before the interaction with the crossed ion beam. The electron current is measured in a biased collector on the opposite side of the interaction region. The electron beam is chopped at a 1 kHz 50% duty cycle to facilitate the measurement of background signal reaching the detector.

The ions emerging from the interaction region are analyzed by a 90° bending magnet. Ions remaining in their incident charge state, q, are collected in a Faraday cup for current measurement while the charge changed ions, $q + 1$, are deflected toward a 90° cylindrical electrostatic analyzer that deflects the signal ions vertically into a particle detector. In Figure 1, the cylindrical analyzer and detector are shown in the same plane as the apparatus for clarity. The signal count rate at a given interaction energy is determined by collecting data with the electron beam on (signal plus background) and off (background) and by subtracting the latter count rate from the former.

The cross sections for each ion discussed here have been measured with both a channel electron multiplier (CEM) detector, with a detection efficiency of 98%, and a high counting rate discrete dynode detector, with a detection efficiency of 90%. Detector efficiencies were verified by comparing results of metastable-free He^+ and C^+ EII measurements to known benchmarks (Peart et al. 1969; Yamada et al. 1989). The later detector replaced the CEM detector as an upgrade to the apparatus enabling larger ion currents to be used in the experiment without significant dead time effects. The resulting cross sections were equivalent using both detectors, at their given efficiencies, and the error weighted averages of the results are presented here as the final experimental values.

The absolute cross section for electron-impact ionization, in the crossed beams geometry, is given by

$$\sigma(E) = \frac{Rqe^2 v_i v_e F}{I_i I_e \left(v_i^2 + v_e^2\right)^{1/2} D}, \tag{1}$$

where R is the background subtracted signal count rate; q is the charge of the incident ion; e is the electron charge; v_i and v_e are the ion and electron velocities, respectively; I_i and I_e are the ion

TABLE 1
ABSOLUTE EXPERIMENTAL UNCERTAINTIES

Source	Uncertainty (%)
Product ion detection and pulse processing	±5
Transmission of product ion to detector	±4
Absolute value of form factor	±4
Ion current measurement	±2
Electron current measurement	±2
Ion velocity	±1
Electron velocity	±1
Quadrature sum	±8.2

NOTE.—These uncertainties are combined with the relative uncertainties at a 90% confidence level to determine the total uncertainty in each data point.

and electron currents, respectively; D is the detection probability of a charge changed ion due to ionization; and F is the overlap form factor of the electron and ion beams. The form factor is determined by

$$F = \frac{\int I_i(z)\,dz \int I_e(z)\,dz}{\int I_i(z) I_e(z)\,dz}, \qquad (2)$$

where $I_i(z)$ and $I_e(z)$ are the measured beam intensity profiles along the direction orthogonal to both beams.

The predominant systematic uncertainties associated with the experiment are listed in Table 1 with the estimated error for each component at a high confidence level (equivalent to a 90% confidence level for statistical uncertainties). These errors are treated as random sign errors, summed in quadrature, and combined with the statistical uncertainty of each data point (at a 90% confidence level) to determine the total uncertainty. These total uncertainties are given in parentheses in Tables 2, 3, and 4. Detailed discussions of the experimental uncertainties have been published previously (Gregory et al. 1983; Bannister 1996).

TABLE 2
ABSOLUTE EXPERIMENTAL CROSS SECTIONS FOR ELECTRON-IMPACT SINGLE IONIZATION OF C^{2+}

E (eV)	σ (10^{-18} cm^2)
38.5	0.17 ± 0.35 (0.58)
42.5	−0.22 ± 0.26 (0.43)
44.3	−0.01 ± 0.39 (0.64)
46.5	1.67 ± 0.29 (0.50)
48.3	1.90 ± 0.25 (0.44)
50.5	2.50 ± 0.24 (0.44)
52.3	3.64 ± 0.22 (0.47)
60.4	6.78 ± 0.65 (1.21)
80.1	10.40 ± 0.19 (0.91)
95.3	12.00 ± 0.15 (1.01)
99.9	11.89 ± 0.34 (1.12)
119.6	11.82 ± 0.25 (1.05)
139.5	12.40 ± 0.18 (1.06)
159.2	11.98 ± 0.36 (1.15)
179.0	11.75 ± 0.50 (1.27)
198.7	11.99 ± 0.23 (1.05)
298.4	10.46 ± 0.51 (1.20)
398.8	8.78 ± 0.43 (1.01)
498.9	7.43 ± 0.27 (0.75)
599.0	6.34 ± 0.30 (0.72)
801.0	3.31 ± 0.11 (0.33)

NOTES.—These data are for an ion beam metastable fraction of 0.46 ± 0.07. The statistical uncertainties are at one standard deviation. The total uncertainties (given in parentheses) are at a high confidence level corresponding to 90% confidence for the statistical uncertainties.

TABLE 3
ABSOLUTE EXPERIMENTAL CROSS SECTIONS FOR ELECTRON-IMPACT SINGLE IONIZATION OF N^{3+}

E (eV)	σ (10^{-18} cm^2)
68.4	0.00 ± 0.04 (0.07)
72.4	0.07 ± 0.07 (0.12)
74.4	0.42 ± 0.04 (0.07)
76.3	0.51 ± 0.04 (0.08)
78.2	0.72 ± 0.06 (0.12)
80.2	0.88 ± 0.03 (0.09)
84.8	1.50 ± 0.04 (0.14)
89.8	1.99 ± 0.04 (0.18)
100.1	2.89 ± 0.14 (0.33)
125.0	3.70 ± 0.10 (0.35)
149.8	4.24 ± 0.11 (0.39)
174.4	4.25 ± 0.13 (0.41)
199.2	4.43 ± 0.13 (0.42)
248.9	4.60 ± 0.23 (0.53)
298.5	4.39 ± 0.13 (0.42)
324.1	4.42 ± 0.09 (0.39)
348.3	4.22 ± 0.07 (0.36)
374.3	4.18 ± 0.05 (0.35)
379.9	4.11 ± 0.10 (0.38)
389.9	3.86 ± 0.07 (0.34)
398.1	4.07 ± 0.07 (0.35)
409.9	3.92 ± 0.07 (0.34)
419.8	3.91 ± 0.08 (0.35)
424.4	3.71 ± 0.04 (0.31)
429.8	3.81 ± 0.08 (0.34)
439.8	3.85 ± 0.07 (0.34)
449.8	3.75 ± 0.04 (0.31)
474.6	3.42 ± 0.07 (0.30)
499.7	3.42 ± 0.04 (0.29)

NOTES.—These data are for an ion beam metastable fraction of 0.30 ± 0.06. The statistical uncertainties are at one standard deviation. The total uncertainties (given in parentheses) are at a high confidence level corresponding to 90% confidence for the statistical uncertainties.

3.2. *Ion Beam Metastable Fraction Determination*

A primary impetus for this study has been to resolve the uncertainty of ion beam metastable states present in previous EII experimental measurements. Most of these measurements made no independent attempt to measure the ion beam metastable fraction directly. One method of measuring the ion beam metastable fraction is the gas attenuation technique (Turner et al. 1968; Vujović et al. 1972; Unterreiter et al. 1991). This method relies on the difference in the electron capture cross sections for ground state and metastable ions. The mixed state ion beam is passed through a gas cell. For a single state ion beam, the ion current of the initial charge state will fall off exponentially proportional to the capture cross section as the attenuating gas pressure is increased. If the ion beam is composed of two different populations, i.e., metastable term and ground state ions with different capture cross sections, then the ion current attenuation will follow the sum of two different exponential decays. If we pick an attenuation gas for which the metastable capture cross section is larger than the ground state capture cross section, then the metastable component of the ion beam will attenuate more rapidly given an increase in attenuation gas pressure

TABLE 4

Absolute Experimental Cross Sections for Electron-Impact Single Ionization of O^{4+}

E (eV)	σ (10^{-18} cm^2)
95.7	0.01 ± 0.03 (0.05)
100.6	0.05 ± 0.03 (0.05)
108.7	0.03 ± 0.02 (0.03)
110.6	0.09 ± 0.02 (0.03)
112.6	0.19 ± 0.03 (0.05)
114.6	0.16 ± 0.03 (0.05)
120.6	0.37 ± 0.02 (0.04)
130.5	0.74 ± 0.03 (0.08)
140.5	1.02 ± 0.02 (0.09)
150.4	1.15 ± 0.03 (0.11)
160.2	1.25 ± 0.02 (0.11)
170.2	1.40 ± 0.04 (0.13)
180.1	1.44 ± 0.03 (0.13)
200.7	1.73 ± 0.04 (0.16)
251.5	1.87 ± 0.05 (0.17)
301.6	2.03 ± 0.03 (0.17)
351.9	1.99 ± 0.03 (0.17)
402.0	1.88 ± 0.03 (0.16)
452.2	1.82 ± 0.03 (0.16)
502.2	1.79 ± 0.03 (0.15)
542.3	1.78 ± 0.03 (0.15)
552.3	1.80 ± 0.02 (0.15)
562.4	1.81 ± 0.02 (0.15)
572.4	1.82 ± 0.02 (0.15)
582.5	1.82 ± 0.03 (0.16)
592.5	1.84 ± 0.03 (0.16)
602.5	1.84 ± 0.02 (0.15)
612.7	1.82 ± 0.02 (0.15)
622.6	1.77 ± 0.02 (0.15)
652.7	1.86 ± 0.04 (0.17)
703.1	1.76 ± 0.05 (0.17)
753.3	1.69 ± 0.05 (0.16)
803.5	1.66 ± 0.02 (0.14)
853.8	1.54 ± 0.03 (0.14)
903.8	1.55 ± 0.02 (0.13)
954.3	1.56 ± 0.05 (0.15)
1004.7	1.54 ± 0.02 (0.13)
1204.6	1.26 ± 0.03 (0.11)
1505.8	1.37 ± 0.03 (0.12)

Notes.—These data are for an ion beam metastable fraction of 0.24 ± 0.07. The statistical uncertainties are at one standard deviation. The total uncertainties (given in parentheses) are at a high confidence level, corresponding to 90% confidence for the statistical uncertainties.

and the ground state exponential decay can be reached at higher gas pressures without significant contribution from the metastable ions. After normalizing the attenuation current measurements to the initial incident current, without gas in the cell, the ground state exponential decay can then be fitted by a simple exponential decay function, $A \exp(-Bx)$, and extrapolated back to zero attenuation gas pressure to determine the ground state ion beam fraction, A, and conversely the metastable fraction, $1 - A$.

The normalized current of the initial charge state is given by

$$\frac{I}{I_0} = (1 - A)\exp(-\sigma_{\rm MS} nl) + A\exp(-\sigma_{\rm GS} nl), \qquad (3)$$

where $\sigma_{\rm MS}$ and $\sigma_{\rm GS}$ are the capture cross sections of metastable term and ground state, respectively, A is the metastable fraction of the ion beam, n is the gas density, and l is the gas cell length.

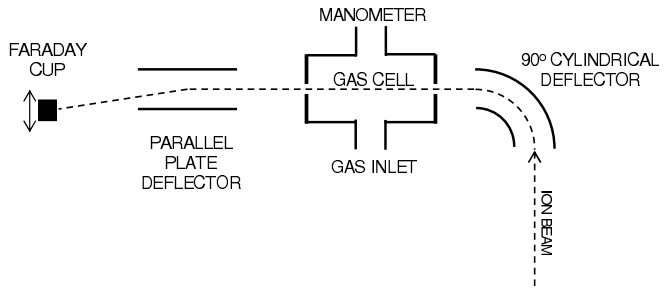

Fig. 2.—Schematic of the gas attenuation apparatus used to measure ion beam metastable fractions. See text for details.

We assume in this model that the cross section for reionization of the $q - 1$ ion, that has captured an electron in the gas cell, is negligible. While the data on projectile ionization cross sections are sparse, Tawara (1992) provides some projectile ionization cross sections for collisions of Be-like ions with atomic hydrogen that are at least an order of magnitude less than the expected capture cross sections of interest in the attenuation technique employed here at the given ion energies. We have modeled the attenuation including refeeding of the initial charge state due to projectile ionization at the given collision energy and conclude that it has a minimal effect on the attenuated ion current, I, over the range of gas cell pressures investigated and is less than the quoted error of our metastable fraction determinations.

Figure 2 shows a schematic of the apparatus used to measure the ion beam metastable fractions via beam attenuation. Helium was chosen as the attenuation gas based on sparsely available capture cross section data (Gardner et al. 1979; Phaneuf et al. 1985; Unterreiter et al. 1991; Ishii et al. 2004), which suggested that the metastable capture cross section, at the experimental ion energies used in this study, were in the range of 3–7 times larger than that of the ground state. It is important to note, however, that these data, with varying levels of metastable contamination, only covered a limited range of energies and provided little information on state-selective capture cross sections. These data only serve as a guide in selecting an attenuation gas and, fortunately, the gas attenuation process used in this study does not rely on the accuracy of these data given that accurate metastable fraction measurements do not require the use of absolute units.

The Be-like ions were analyzed by a 90° electrostatic cylindrical deflector to remove any ions that could have undergone charge exchange with the residual gas in the beam line between the ion source and the gas attenuation apparatus. The ions were then passed through a 25 cm long gas cell with a 3 mm diameter entrance aperture and a 6 mm diameter exit aperture. The ions were subsequently analyzed by a parallel plate deflector so that the initial Be-like ion beam current could be measured in a Faraday cup. Ions undergoing capture in the gas cell would not reach the Faraday cup and would result in ion current loss. The ion current was measured as a function of gas cell pressure, which ranged from approximately 0–10 mTorr, as measured with a Baratron capacitive manometer. It is worth noting that the ion current and pressure measurements do not require calibration and can be made in arbitrary units as long as a linear instrument response function persists over the full measurement range. This greatly simplifies the measurement of metastable fractions via the gas attenuation technique. Figure 3 illustrates the normalized ion beam current of C^{2+} as a function of gas cell pressure. Fits to the attenuation data at high pressure are extrapolated back to zero gas cell pressure to determine the ion beam ground state and metastable term fractions. For C^{2+}, the ion beam metastable fraction was determined to be

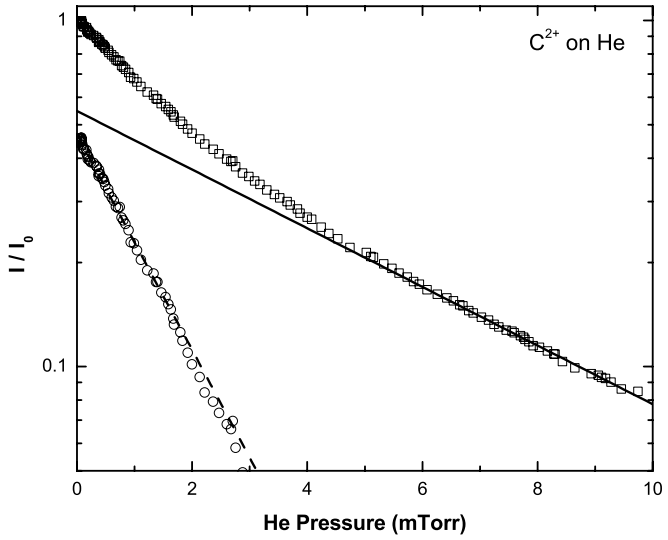

FIG. 3.—Beam attenuation of C^{2+} ions by He gas. The open squares show the normalized ion current of C^{2+} as a function of attenuation gas cell pressure. The solid line is a fit to the high-pressure region where the attenuation is predominantly due to ground state ions. The open circles show the residuals of the C^{2+} attenuation minus the fit. This represents the pure metastable attenuation. The dashed curve is a fit to the pure metastable attenuation. The fit values at zero gas pressure give the ground and metastable ion beam fractions.

0.46 ± 0.07 (at a 90% confidence level). This type of attenuation measurement and fit was also made for N^{3+} and O^{4+}, in which respective ion beam metastable fractions of 0.30 ± 0.06 and 0.24 ± 0.07 were determined. Consequently, the deduced metastable-to-ground capture cross section ratios were approximately 3.5, 1.5, and 1.8, respectively for C^{2+}, N^{3+}, and O^{4+} at the given ion energy of $10q$ keV. These values are less than what was estimated from the capture cross section data mentioned above.

4. THEORY

For the EII of atoms and ions, the total ionization cross section is given by

$$\sigma_{\text{total}} = \sum_i \sigma_{\text{direct}} + \sum_j \sigma_{\text{EA}}, \tag{4}$$

where the sum i is over the direct ionization channels, and the sum j is over the inner subshell electrons, which can be excited, leading to an autoionizing configuration. The excitation-autoionization contribution to the total ionization cross section is given by

$$\sigma_{\text{EA}}(j) = \sum_k \sigma_{\text{exc}}(j \rightarrow k) B_k^a, \tag{5}$$

where $\sigma_{\text{exc}}(j \rightarrow k)$ is the excitation cross section from a term j of the initial configuration to a term k of the final excited configuration. The branching ratio for autoionization, B_k^a, from the term k is the ratio of the total Auger rates to the total Auger and radiative rates from the term k. For the light Be-like ions investigated here the autoionization rates are far greater than the radiative rates, leading to unity branching ratios.

4.1. *Configuration-Average Distorted-Wave*

The theory for the time-independent, configuration-average, distorted-wave (CADW) method has been described in detail previously by Pindzola et al. (1986). The configuration-average threshold energies and radial wave functions for the bound configurations are evaluated using the Hartree-Fock semirelativistic atomic structure code of Cowan (1981).

The direct ionization cross section contributions to the total cross section are calculated in a CADW approximation. Consider the transition

$$(nl)^{\omega} k_i l_i \rightarrow (nl)^{\omega-1} k_e l_e k_f l_f, \tag{6}$$

where ω is the occupation number of the initial subshell being ionized, $k_i l_i$ are the quantum numbers of the incident electron, while $k_e l_e$ and $k_f l_f$ are the quantum numbers for the ejected and final continuum electrons, respectively. The configuration-average direct cross section is given by

$$\sigma_{\text{direct}} = \frac{32\omega}{k_i^3} \int_0^{E/2} \frac{d\left(k_e^2/2\right)}{k_e k_f} \times \sum_{l_i, l_e, l_f} (2l_i+1)(2l_e+1)\left(2l_f+1\right)\mathcal{P}\left(l_i, l_e, l_f, k_i, k_e, k_f\right), \tag{7}$$

where $\mathcal{P}$ is the first-order scattering probability and has previously been described in more detail (Pindzola et al. 1986).

Using the angular branching factors of Sampson (1986) it is possible to resolve the initial and final configurations into their terms or levels for the direct ionization cross sections. Thus, the CADW results to be presented here will be split into term-resolved cross sections. As part of this process the term-resolved cross sections are shifted so that the calculated threshold agrees with spectroscopic values taken from the NIST database (NIST 2007). As a check on our splitting of the CADW results into term-resolved cross sections, we performed a term-resolved distorted-wave calculation for the ionization of the $2s2p$ configuration of N^{3+}. The cross sections calculated using the term-resolved DW code were extremely close to those of the CADW calculation with the appropriate angular factors applied.

For all the Be-like ions studied here direct ionization of the $1s$ shell will leave the ion in an autoionizing term, for which the Auger yield will be very close to unity. Thus, direct ionization of a $1s$ electron will in fact lead to a double ionization of the Be-like ion. For this reason we do not include any direct ionization from the $1s$ shell in our calculations.

The excitation cross sections used in excitation-autoionization cross section calculations can also be evaluated in a CADW approximation. In this approach, the excitation process is represented by

$$(n_1 l_1)^{\omega_1+1} (n_2 l_2)^{\omega_2-1} k_i l_i \rightarrow (n_1 l_1)^{\omega_1} (n_2 l_2)^{\omega_2} k_f l_f, \tag{8}$$

where $n_1 l_1$ and $n_2 l_2$ are quantum numbers of the bound electrons, and $k_i l_i$ and $k_f l_f$ are quantum numbers of the initial and final continuum electrons, respectively. The configuration-average excitation cross section is given by

$$\sigma_{\text{exc}} = \frac{8\pi}{k_i^3 k_f}(\omega_1+1)(4l_2+3-\omega_2) \times \sum_{l_i, l_f} (2l_i+1)\left(2l_f+1\right)\mathcal{P}\left(l_i, l_f, k_i, k_f\right), \tag{9}$$

where $\mathcal{P}$ is the first-order scattering probability (Pindzola et al. 1986). In this work we assume that the Auger yields of autoionizing configurations are unity. Thus, excitation of the $1s$ shell to autoionizing configurations is assumed to lead to a single ionization

TABLE 5
RMPS EII Cross Section Fitting Parameters Using the Rost & Pattard (1997) Model for Energies up to 2000 eV[a]

Parameter	C^{2+} ($2s^2\ ^1S$)	C^{2+} ($2s2p\ ^3P$)	N^{3+} ($2s^2\ ^1S$)	N^{3+} ($2s2p\ ^3P$)	O^{4+} ($2s^2\ ^1S$)	O^{4+} ($2s2p\ ^3P$)
Ionization potential (eV)	47.89	41.40	77.47	69.14	113.90	103.74
$E_m^{(\alpha)}$ (eV)	66.9237	39.9406	94.7662	56.2042	142.995	113.283
$\sigma_m^{(\alpha)}$ (10^{-18} cm^2)	9.3975	12.6069	3.88517	4.77283	1.91116	2.43434
$E_m^{(3\alpha)}$ (eV)	147.936	86.8495	212.425	124.928	331.961	251.883
$\sigma_m^{(3\alpha)}$ (10^{-18} cm^2)	4.50841	10.6914	2.03244	4.55683	0.88264	1.31352

[a] For ease of use of our data we provide a FORTRAN code at http://www-cfadc.phy.ornl.gov/data_and_codes that can be used to generate rate coefficients from the fitting parameters above.

for the ground and metastable initial terms. Also, excitation of a $2s$ subshell electron from the $2s2p\ ^3P$ metastable term to an autoionizing configuration is assumed to lead to a single ionization.

The CADW method described above has been successful in evaluating ionization cross sections, particularly for ionized species (Loch et al. 2002). However, the method often does not do well for near neutral species or excited states, as was seen previously for C^{2+} (Loch et al. 2005a) and H (Griffin et al. 2005).

4.2. *R-Matrix With Pseudostates*

The *R*-matrix with pseudostates (RMPS) method has been described in detail previously (see Bartschat 1998; Mitnik et al. 1999, 2003). Our implementation of this method employs a set of Laguerre radial wave functions to represent the high Rydberg states and the target continuum. One determines the ionization cross section by summing over the positive energy pseudostates above the first ionization limit. All radial functions employed in this calculation were generated using the program AUTOSTRUCTURE (Badnell 1997).

Spectroscopic orbitals were employed for all subshells from $1s$ to $4f$ for C^{2+} and from $1s$ to $3d$ for N^{3+} and O^{4+}. These orbitals were determined from a local potential using Slater-type orbitals. A set of nonorthogonal Laguerre pseudo-orbitals was generated for all subshells from $5s$ to $14g$ for C^{2+} and from $4s$ to $14g$ for N^{3+} and O^{4+}. These pseudo orbitals were then orthogonalized to the spectroscopic orbitals and to each other. The close-coupling expansion of the target included all terms of the configurations $2s^2$, $2s2p$, $2p^2$, $2snl$ with $n = 3$ to 14 and $l = 0$ to 4, and $2pnl$ with $n = 3$ to 14 and $l = 0$ to 4, leading to a total of 414 terms. Note that this allows for direct ionization of both the $2s$ and $2p$ electrons from the $2s2p$ configuration.

The RMPS calculation was performed using our recently developed set of parallel *R*-matrix codes (see Mitnik et al. 1999; Ballance & Griffin 2004). For C^{2+} an RMPS calculation with exchange was performed for all $LS\Pi$ partial waves from $L = 0$ to 13. This was then supplemented by a no-exchange calculation from $L = 13$ to 20, and higher L values were included using a top-up procedure. For N^{3+} and O^{4+} our exchange calculation included all $LS\Pi$ partial waves (of the $N + 1$ system) from $L = 0$ to 13. The effects of the higher partial waves were included using a top-up procedure, but were found to be negligible for both of these ions for the energy range over which our RMPS calculation extended. For C^{2+} we employed 50 basis orbitals to represent the $(N + 1)$-electron continuum for each value of the angular momentum. For N^{3+} and O^{4+} we used 38 basis orbitals.

The most important part of the ionization cross section is the part just above the ionization threshold. The critical ionization rate coefficients are at electron temperatures below the ionization potential. For example, for C^{2+} with an ionization potential of 47.89 eV a collisional ionization equilibrium calculation predicts greater than 1% fractional abundance for a temperature range of 2–15 eV (Bryans et al. 2006). For this reason, our RMPS cross sections were fitted using the expression of Rost & Pattard (1997). This expression has the correct threshold behavior for the cross section, following the Wannier theory threshold scaling (Wannier 1953).

We used equation (4) from Rost & Pattard (1997) in our fitting. We fixed the ionization potential and used $E_m^{(\alpha)}$, $\sigma_m^{(\alpha)}$, $E_m^{(3\alpha)}$, $\sigma_m^{(3\alpha)}$ as our free parameters in the fit to the RMPS raw data. These four variables correspond to the variables with the same notation in Rost & Pattard (1997). That is, $E_m^{(\alpha)}$ and $\sigma_m^{(\alpha)}$ are the energy and cross section value of the peak of the α contribution, and $E_m^{(3\alpha)}$ and $\sigma_m^{(3\alpha)}$ are the energy and cross section value of the peak of the 3α contribution to the total cross section. Good fits were achieved for all RMPS cross sections, with typical rms errors of 3% in the fits. Our fitting parameters are given in Table 5.

We also performed least-squares fits to the RMPS cross sections using the expression of Younger (1981a). This fit was fixed at the ionization threshold and the Bethe high-energy limit was used from a configuration-average photo-ionization calculation. However, this fit did not give the required accuracy at low energies as has been pointed out previously by Pindzola et al. (1996). Thus, we only show results from the fit using the expression of Rost & Pattard (1997).

One must fit the RMPS results for a number of reasons. Since the continuum is represented by a finite number of pseudostates there are oscillations in the RMPS ionization cross section. In our cases these oscillations are very small, due to the large number of pseudostates involved. But a fit to the RMPS data ensures that these pseudostate oscillations are smoothed out. Also, the RMPS calculation extends up to about 250–300 eV for each of the ions studied. Thus, to produce rate coefficients, we require a fit that will extend the RMPS results up to higher energies. The Rost & Pattard (1997) fit suits our purposes well, as it ensures the right threshold behavior and can extend our RMPS results to higher energy.

One issue of using the Rost & Pattard fit is that it has a classical high-energy slope instead of a quantum result, i.e., $1/E$ instead of $\ln(E)/E$. To make sure that we were not being affected by this we checked the upper limit on our rate coefficient integral such that the rate coefficient is converged to 99% of its value. We found that all of our rate coefficients had converged before the high-energy trend of the Rost & Pattard fit would be a problem.

It should be noted that the RMPS calculations were significantly more computationally intensive for C^{2+}, compared with the calculations for the other two ions. In all cases we had to use massively parallel computers for the calculations. For C^{2+} the larger basis set, which was required to represent the $(N + 1)$-electron system, led to much larger matrices to be diagonalized, often with a size of $64{,}000 \times 64{,}000$. Thus, we note that the RMPS calculations reported here are significantly larger calculations than those reported earlier in Loch et al. (2005a) and have allowed us to

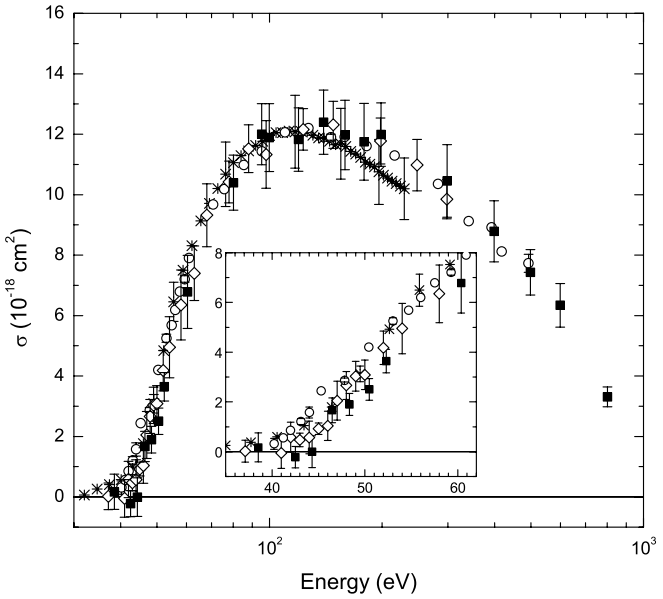

FIG. 4.—Experimental measurements for the absolute EII cross sections of C^{2+}. The solid squares represent the current experimental work, the open diamond symbols are the data of Woodruff et al. (1978), the open circle symbols are the data of Falk et al. (1983), and the star symbols are the data of Loch et al. (2005a).

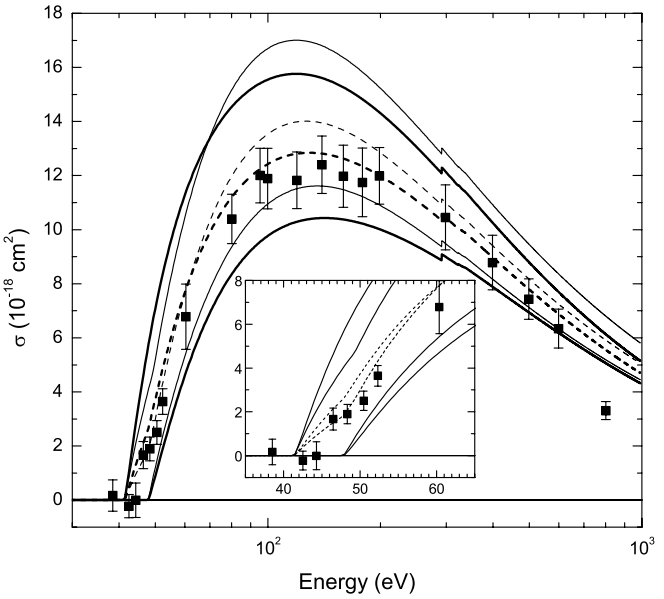

FIG. 5.—Current experimental measurements for C^{2+} (*filled squares*) are compared with CADW (*thin solid curves*) and RMPS (*thick solid curves*) theoretical cross sections for both ground state (*bottom solid curves*) and metastable term (*top solid curves*) ions. The dashed curves of each line type represent the admixture of ground state and metastable term cross sections at the experimentally inferred ion beam metastable fraction of 0.46.

test the convergence of those previous calculations. The new calculation has been extended to higher energies, and produces slightly higher cross section values at the peak of the cross section. This difference is due largely to the increased basis set. Various RMPS calculations were performed for C^{2+} to test convergence. We investigated the size of the basis set, the number of pseudostates, and the *n*-shell to which we topped up the *R*-matrix results. For each of these parameters the final cross section results were found to have converged. We also note that the new RMPS results are in good agreement with previous TDCC and CCC calculations (Loch et al. 2005a).

5. RESULTS AND DISCUSSION

5.1. $C^{2+} \rightarrow C^{3+}$

Our experimental C^{2+} EII cross section data and uncertainties are given in Table 2. Figure 4 shows the present measurements of the C^{2+} EII cross sections, with a metastable fraction of 0.46 ± 0.07, compared with the measurements of Woodruff et al. (1978), Falk et al. (1983), and Loch et al. (2005a). Woodruff et al. do not give a metastable fraction estimation; Falk et al. estimate their metastable fraction to be 0.65; and Loch et al. estimate their metastable fraction to be 0.60. As can be seen from Figure 4, all of the results are within experimental uncertainty of each other. However, it should be noted that not all of the experimental results are reported with the same confidence levels. The inset of Figure 4 shows that this agreement extends down to the ground state and metastable term thresholds of 47.9 and 41.4 eV, respectively. Although the various experiments have similar metastable fractions, it should be cautioned that the range of total absolute uncertainty in the data can easily be explained by metastable fractions spanning from 0.15–0.75 when using the RMPS predictions. This emphasizes the importance of determining the metastable fraction by some other means, such as the gas attenuation method used here, instead of attempting to fit theoretical models to the EII data.

Figure 5 shows the current experimental EII cross sections compared to both our CADW and the RMPS theoretical results. The two different sets of solid curves in Figure 5 represent the ground state and metastable term. In both the CADW and the RMPS total cross section results, excitation-autoionization was calculated using the CADW method. For ionization from the $1s^2 2s^2$ ground configuration, excitation of the 1*s* shell leads to a small excitation-autoionization contribution starting at about 290 eV. This contribution is too small for observation given the level of uncertainty in the experiment. For the $2s2p\ ^3P$ metastable term, the first autoionizing configuration fully accessible via excitation of a 2*s* electron is the $1s^2 2p4f$ configuration. According to energies listed on the NIST database (NIST 2007) the levels of the $1s^2 2p4d$ configuration straddle the metastable ionization threshold. We do not include the contribution from the $1s^2 2p4d$ configuration in our excitation-autoionization calculations.

The dashed curves in Figure 5 represent the mixed ground and metastable contributions at the metastable fraction measured using the gas attenuation technique. We note that there is overall good agreement between the mixed ground and metastable RMPS results and the experimental measurements over most of the energy range investigated. In the near threshold region, the mixed RMPS results are slightly higher than the current experimental measurements, while the mixed CADW results tend to agree better over this limited range of energies between the ground and metastable thresholds. However, CADW clearly overestimates the peaks of the cross sections for both the ground and metastable configurations as was pointed out previously by Loch et al. (2005a). We should mention that the RMPS metastable cross sections have both a 2*s* and a 2*p* contribution that cannot be distinguished due to configuration interaction mixing between pseudostate terms. This causes a smoothing of the RMPS metastable cross section in the near threshold region. Our mixed RMPS cross sections produce the best overall agreement with the experimental measurements. Therefore, the pure ground and metastable RMPS cross sections represent our recommended EII cross section data.

In comparing our recommended ground state RMPS cross section for C^{2+} to the previous theoretical results of Moores (1978) and Jakubowicz & Moores (1981) mentioned in § 2.1, we find that

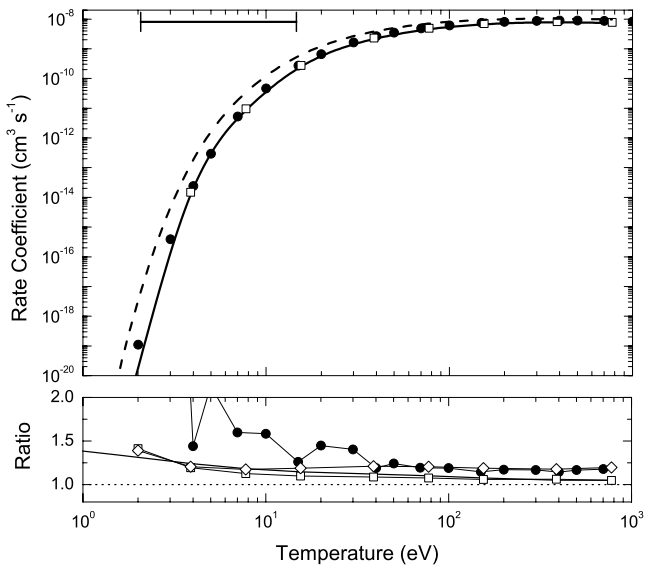

FIG. 6.—*Top*: Maxwellian rate coefficients for EII of C^{2+}. The thick solid curve represents the pure ground state RMPS results, the filled circles represent the rate coefficient recommended by Bell et al. (1983), and the open squares represent the rate coefficient recommended by Arnaud & Rothenflug (1985). The dashed curve represents the RMPS rate coefficient for the pure metastable $2s2p\ ^3P$ term. The temperature range for >1% fractional abundance in the CIE regime is shown by the horizontal line at the top of the plot (Bryans et al. 2006). The data of Dere (2007) are not plotted in the top panel for clarity. *Bottom*: Ratio relative to the ground state RMPS rate coefficient for our CADW results (*solid curve*), the Bell et al. (1983) data (*filled circles*), the Arnaud & Rothenflug (1985) data (*open squares*), and the Dere (2007) data (*open diamonds*). The lines interconnecting symbols are only meant to guide the eye.

the Coulomb-Born calculations of Moores (1978) are approximately 26% larger at the peak of the cross section, while the distorted Coulomb-Born with exchange (DCBX) calculations of Jakubowicz & Moores (1981) are approximately 18% larger.

We have generated our recommended Maxwellian rate coefficients using the RMPS cross section results. Figure 6 shows our recommended data, for both pure ground and metastable terms, compared with rate coefficients archived in the literature. The range over which the fractional abundance of C^{2+} is greater than 1% in the CIE regime is indicated at the top of the figure (Bryans et al. 2006). This covers a temperature range of approximately 2–15 eV. The bottom panel of Figure 6 gives the ratio of our CADW results and the data of Bell et al. (1983), Arnaud & Rothenflug (1985), and Dere (2007) to the recommended ground state RMPS rate coefficient. As can be seen from these ratios, the Bell et al. data average more than 50% higher than the RMPS data in the CIE region. The Arnaud & Rothenflug data closely follow that of our CADW, which can be as much as 40% higher than the RMPS rate coefficients at the low end of the region of fractional abundance. The Dere (2007) data is approximately 17%–20% higher than the RMPS data over the entire temperature range and agrees with both CADW and Arnaud & Rothenflug in the CIE region.

It is interesting to note that, in the CIE region, the rate coefficient is strongly dependent on the near threshold portion of the EII cross section. We have investigated how much of the EII cross section, above threshold, is required to converge to 99% of our current results when convoluting the cross section with a Maxwellian distribution to form the rate coefficients. Expressing the results in terms of the Maxwellian electron temperature T_e and ionization potential $I_{\rm eV}$ of the given term, we find that we need to include the portion of the cross section from $I_{\rm eV}$ to approximately $6T_e + I_{\rm eV}$ in producing a Maxwellian rate coefficient at a given temperature T_e (in units of eV), e.g., for ground state C^{2+}, at the upper temperature limit of the CIE region, the cross section up to approximately 138 eV is needed to converge to 99% of the Maxwellian rate coefficient. This result basically stems from the functional form of the EII cross section and seems to only hold true for cases in which there is no significant variation of that form in the region between the ionization potential and the peak of the cross section, i.e., no significant excitation-autoionization contributions. We have also verified that our current rate coefficients have indeed converged with respect to the step size used to convolute the EII cross section.

In the high electron temperature region, $k_{\rm B}T_e > 100$ eV, the Bell et al. data are approximately 14%–18% higher than the RMPS rate coefficients, while the CADW and Arnaud & Rothenflug results are approximately 5%–7% higher. The rate coefficients of Dere (2007) agree with the Bell et al. data in the high-temperature region. Given that this temperature range is far above the CIE fractional abundance region, these data would probably be of more interest to nonequilibrium systems. At these temperatures, knowledge of the high-energy portions of the EII cross section is required, and we observe that our simple formula given above is still valid in determining how much of the cross section is needed in producing a reliable Maxwellian rate coefficient at a given temperature $k_{\rm B}T_e$. A caveat would be that a Maxwellian temperature distribution may not provide the best means of describing such nonequilibrium systems. In order to use our recommended EII cross sections for non-Maxwellian modeling, we have provided our RMPS cross section fitting parameters, using the model of Rost & Pattard (1997) in Table 5. Since the Rost & Pattard fits to our RMPS cross sections are based on the threshold ionization potentials and the peak values of the cross sections, we can obtain a reasonable estimate of the uncertainties in our final rate coefficients by considering the uncertainties in our benchmark experimental measurements at the peak of the cross sections. These errors can be gauged from the total uncertainties given in Tables 2, 3, and 4. However, one must be careful to control the fit error to the cross sections as inappropriate fitting of the near threshold region can lead to significant uncertainties in the low-temperature rate coefficients.

It is also worth noting that, given the long lifetime of the metastable state, it may be important to include ionization from the metastable state in a given model. For this purpose, we have generated a Maxwellian rate coefficient curve for the pure $2s2p\ ^3P$ metastable term, shown as a thick dashed curve in Figure 6, from our metastable RMPS cross section results. However, as pointed out above, the near threshold region of the metastable RMPS cross section does not differentiate between the $2s$ and $2p$ thresholds due to pseudostate mixing and may not exhibit the correct threshold behavior. Since the low-temperature rate coefficient strongly depends on the shape of the cross section near threshold, this may have the effect of elevating the rate coefficient in the low-temperature region while having a negligible effect in the high-temperature region, where the contribution of metastable ionization may be more important in nonequilibrium systems.

Using our calculated RMPS Maxwellian rate coefficients, we have produced a set of fitting coefficients so that the rate coefficients can be easily reproduced in modeling codes. We tried various fitting functions; however, given that the rate coefficients spanned several orders of magnitude over the temperature range of interest, it was difficult to isolate a fitting function that performed well over such a large range. The expression of Younger (1981b) was initially used to fit the resulting rate coefficients, but it was found that it did not give the required accuracy across the

TABLE 6
Fifth-Order Polynomial Fitting Parameters Used to Reproduce Scaled RMPS Rate Coefficients

Ion	Ionization Potential (eV)	a_0	a_1	a_2	a_3	a_4	a_5
C^{2+} ($2s^2\ ^1S$)	47.89	-1.25771×10^{-6}	3.90626×10^{-5}	-1.30284×10^{-4}	2.16906×10^{-4}	-1.72776×10^{-4}	5.28348×10^{-5}
C^{2+} ($2s2p\ ^3P$)	41.40	-1.44181×10^{-6}	4.92601×10^{-5}	-1.42876×10^{-4}	1.88860×10^{-4}	-1.07054×10^{-4}	1.75093×10^{-5}
N^{3+} ($2s^2\ ^1S$)	77.47	-1.40809×10^{-6}	4.49413×10^{-5}	-1.40303×10^{-4}	2.13297×10^{-4}	-1.51508×10^{-4}	3.93969×10^{-5}
N^{3+} ($2s2p\ ^3P$)	69.14	-1.46840×10^{-6}	5.63484×10^{-5}	-1.50095×10^{-4}	1.63550×10^{-4}	-5.44708×10^{-5}	-9.80484×10^{-6}
O^{4+} ($2s^2\ ^1S$)	113.90	-1.4155×10^{-6}	4.5942×10^{-5}	-1.4289×10^{-4}	2.1727×10^{-4}	-1.5445×10^{-4}	4.0084×10^{-5}
O^{4+} ($2s2p\ ^3P$)	103.74	-1.2819×10^{-6}	4.8368×10^{-5}	-1.3010×10^{-4}	1.5245×10^{-4}	-6.3300×10^{-5}	-1.8588×10^{-6}

Note.—See text for usage details.

whole temperature range of the rate coefficients; tending to fit the high-temperature region better. The most successful fit was achieved using the scaled temperatures and rate coefficients model as reported by Dere (2007). This is similar to the Burgess & Tully (1992) scaling of excitation rate coefficients. The temperatures were scaled as

$$x = 1 - \frac{\ln f}{\ln(t + f)}, \tag{10}$$

and the rate coefficients were scaled as

$$\rho = t^{1/2} I_{\rm eV}^{3/2} R(k_{\rm B} T_e)/E_1(1/t), \tag{11}$$

where $t = k_{\rm B} T_e / I_{\rm eV}$, $I_{\rm eV}$ is the ionization potential ($k_{\rm B} T_e$ and $I_{\rm eV}$ given in eV), $R(k_{\rm B} T_e)$ is the unscaled rate coefficient ($\rm cm^3\ s^{-1}$) and $E_1(1/t)$ is the first exponential integral. f is a scaling parameter in which a value of 1.1 was used for all of our fits as this gave good resolution of the low-temperature rate coefficients.

These scaled quantities were fitted with a fifth-order polynomial. The fitting parameters are presented in Table 6 and correspond to scaled rate coefficients given by

$$\rho = a_0 + a_1 x + a_2 x^2 + a_3 x^3 + a_4 x^4 + a_5 x^5. \tag{12}$$

Note that to use the fitting parameters one must first evaluate the desired scaled temperature using equation (10), then use the fitting parameters in Table 6 with equation (12) above to generate the scaled rate coefficients. This then needs to be converted into an unscaled rate coefficient by rearranging equation (11) to solve for $R(k_{\rm B} T_e)$. For C^{2+}, the error in our fit was less than 3% for the ground state rate coefficient and less than 4% for the metastable state rate coefficient. For much of the temperature range, the error was less than 2%. The uncertainty in the rate coefficients generated from the polynomial fits are predominately governed by the experimental uncertainties to which we have benchmarked the RMPS cross section calculations. The total experimental uncertainties in Tables 2, 3, and 4 directly reflect the rate coefficient uncertainties derived from the RMPS results.

Table 7 gives the Maxwellian temperature versus our recommended RMPS EII rate coefficients, given as $\log_{10}$ decimal exponents, for both the ground state and metastable term of the ions investigated. These values are generated directly from the convolution of the RMPS cross sections with a Maxwellian distribution. This provides an alternative means of data reproduction to the fitted rate coefficients and can be used to suit specific application needs.

5.2. $N^{3+} \rightarrow N^{4+}$

Our experimental N^{3+} EII cross section data and uncertainties are given in Table 3. Figure 7 shows the present measurements of the N^{3+} EII cross sections, with a metastable fraction of 0.30 ± 0.06, compared with the measurements of Falk et al. (1983). Falk et al. estimate a metastable fraction of 0.90 in their ion beam. Our cross section measurements are consistently lower than the Falk et al. values, indeed suggesting a lower metastable fraction in our beam. As can be seen in the inset of Figure 7, this discrepancy extends down to the ground state and metastable term thresholds of 77.5 and 69.2 eV, respectively.

Figure 8 shows our current experimental EII cross sections compared with the CADW and the RMPS theory results, assuming a 0.30 metastable fraction. The excitation-autoionization contribution was calculated using the CADW method. For N^{3+}, excitation of a $1s$ electron makes a small contribution to the ionization cross section for both the ground and metastable cross sections. For both the ground and metastable terms the $1s$ EA contribution starts near 410 eV, and is not observed in the experimental data. For the $2s2p\ ^3P$ metastable term, the first autoionizing configuration accessible via excitation of a $2s$ electron is the $1s^2 2p6s$ configuration.

The dashed curves in Figure 8 represent the mixed ground and metastable contributions at the metastable fraction measured using the gas attenuation technique. We note that there is overall good agreement between the mixed ground and metastable RMPS results and the experimental measurements over most of the energy range investigated. In the region near the peak of the cross section, we note that both the RMPS and the CADW results are slightly higher than the current experimental results with the CADW being highest. In the near threshold region, the mixed RMPS and the mixed CADW results tend to agree with each other, however, they are both slightly higher than the observed experimental values. This, again, could partially be due to the fact that the RMPS metastable theory results have some uncertainty in the threshold region due to pseudostate mixing. The RMPS results represent our recommended EII cross sections. Our recommended cross sections can be reproduced using the Rost & Pattard (1997) fitting model parameters given in Table 5.

In comparing our recommended ground state RMPS cross section for N^{3+} to the no-exchange Coulomb-Born calculations of Moores (1978) we find that the cross section of Moores is approximately 15% larger at the peak of the cross section. The distorted Coulomb-Born with exchange calculations of Jakubowicz & Moores (1981) are approximately 12% larger at the peak of the cross section.

We have generated our recommended Maxwellian rate coefficients using the pure ground and metastable RMPS cross section results. Figure 9 shows our recommended data, for both the ground state and metastable term, compared with rate coefficients archived in the literature. The range over which the fractional abundance of N^{3+} is greater than 1% in the CIE regime is given at the top of the figure (Bryans et al. 2006). This covers a temperature range

TABLE 7

RECOMMENDED RMPS EII RATE COEFFICIENTS ($\log_{10}$ cm^3 s^{-1})

$\log_{10}T_e$ (eV)	C^{2+} ($2s^2\ ^1S$)	C^{2+} ($2s2p\ ^3P$)	N^{3+} ($2s^2\ ^1S$)	N^{3+} ($2s2p\ ^3P$)	O^{4+} ($2s^2\ ^1S$)	O^{4+} ($2s2p\ ^3P$)
0.1	−25.4032	−22.8531	−36.0444	−32.8663	−49.0883	−45.3686
0.2	−21.9226	−19.8428	−30.4355	−27.8605	−40.8531	−37.8668
0.3	−19.1496	−17.4447	−25.9740	−23.8788	−34.3072	−31.9033
0.4	−16.9383	−15.5328	−22.4229	−20.7102	−29.1021	−27.1607
0.5	−15.1731	−14.0072	−19.5946	−18.1871	−24.9610	−23.3870
0.6	−13.7622	−12.7889	−17.3399	−16.1769	−21.6641	−20.3823
0.7	−12.6331	−11.8150	−15.5409	−14.5741	−19.0375	−17.9881
0.8	−11.7282	−11.0357	−14.1039	−13.2954	−16.9429	−16.0788
0.9	−11.0019	−10.4115	−12.9549	−12.2745	−15.2709	−14.5548
1.0	−10.4181	−9.9109	−12.0350	−11.4588	−13.9348	−13.3373
1.1	−9.9481	−9.5089	−11.2977	−10.8066	−12.8660	−12.3636
1.2	−9.5692	−9.1856	−10.7061	−10.2846	−12.0100	−11.5841
1.3	−9.2634	−8.9252	−10.2308	−9.8664	−11.3235	−10.9597
1.4	−9.0163	−8.7152	−9.8487	−9.5309	−10.7726	−10.4589
1.5	−8.8164	−8.5458	−9.5411	−9.2613	−10.3299	−10.0571
1.6	−8.6547	−8.4092	−9.2933	−9.0446	−9.9739	−9.7345
1.7	−8.5241	−8.2995	−9.0936	−8.8703	−9.6875	−9.4753
1.8	−8.4188	−8.2119	−8.9327	−8.7303	−9.4569	−9.2670
1.9	−8.3344	−8.1428	−8.8032	−8.6181	−9.2713	−9.0999
2.0	−8.2675	−8.0893	−8.6993	−8.5289	−9.1221	−8.9659
2.1	−8.2153	−8.0491	−8.6165	−8.4589	−9.0023	−8.8590
2.2	−8.1756	−8.0205	−8.5513	−8.4050	−8.9064	−8.7742
2.3	−8.1467	−8.0019	−8.5007	−8.3648	−8.8304	−8.7077
2.4	−8.1272	−7.9920	−8.4626	−8.3365	−8.7707	−8.6567
2.5	−8.1160	−7.9898	−8.4353	−8.3183	−8.7248	−8.6186
2.6	−8.1122	−7.9944	−8.4174	−8.3091	−8.6906	−8.5918
2.7	−8.1148	−8.0049	−8.4078	−8.3076	−8.6665	−8.5745
2.8	−8.1233	−8.0206	−8.4053	−8.3129	−8.6512	−8.5657
2.9	−8.1369	−8.0409	−8.4093	−8.3242	−8.6437	−8.5642
3.0	−8.1551	−8.0653	−8.4190	−8.3408	−8.6430	−8.5692

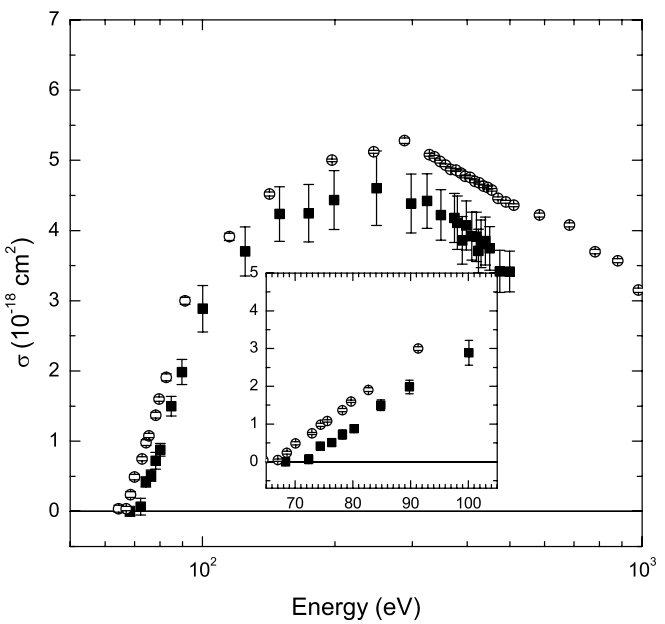

FIG. 7.—Experimental measurements for the absolute EII cross sections of N^{3+}. The solid squares represent the current experimental work, the open circles are the data of Falk et al. (1983).

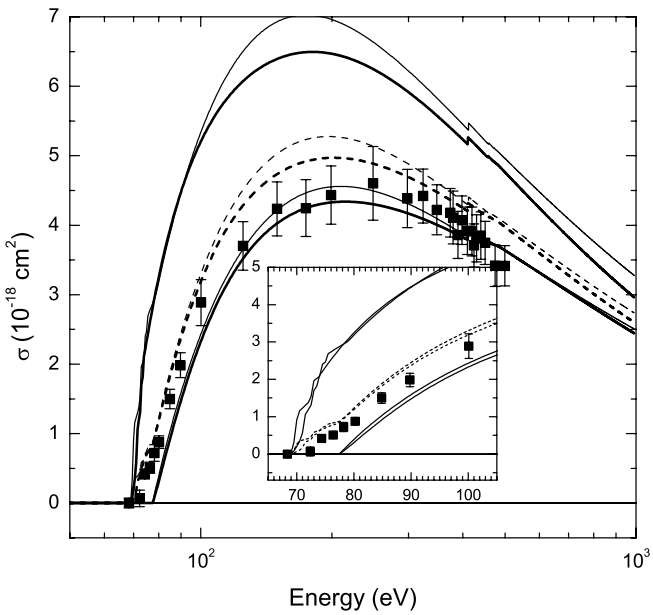

FIG. 8.—Current experimental measurements for N^{3+} (*filled squares*) are compared with CADW (*thin solid curves*) and RMPS (*thick solid curves*) theoretical cross sections for both ground state (*bottom solid curves*) and metastable term (*top solid curves*) ions. The dashed curves of each line type represent the admixture of ground state and metastable term cross sections at the experimentally inferred ion beam metastable fraction of 0.30.

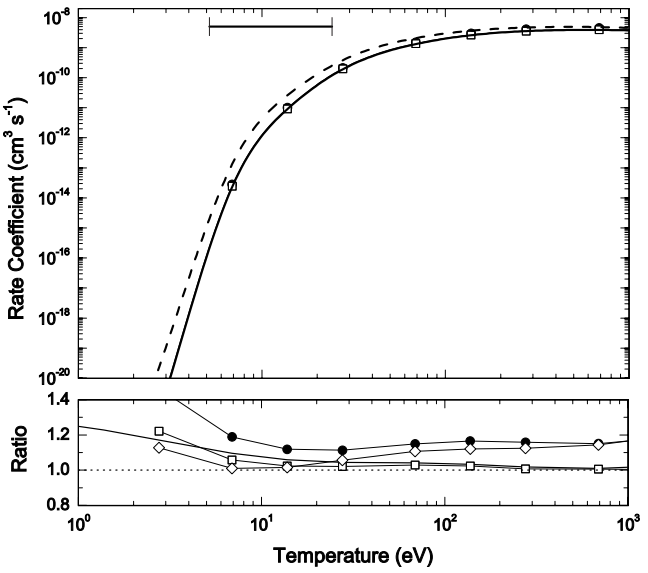

FIG. 9.—*Top*: Maxwellian rate coefficients for EII of N^{3+}. The thick solid curve represents the pure ground state RMPS results, the filled circles represent the rate coefficient recommended by Bell et al. (1983) and the open squares represent the rate coefficient recommended by Arnaud & Rothenflug (1985). The dashed curve represents the RMPS rate coefficient for the pure metastable $2s2p\ ^3P$ term. The temperature range for >1% fractional abundance in the CIE regime is shown by the horizontal line at the top of the plot (Bryans et al. 2006). The data of Dere (2007) are not plotted in the top panel for clarity. *Bottom*: Ratio relative to the ground state RMPS rate coefficient for our CADW results (*solid curve*), the Bell et al. (1983) data (*filled circles*), the Arnaud & Rothenflug (1985) data (*open squares*), and the Dere (2007) data (*open diamonds*). The lines interconnecting symbols are only meant to guide the eye.

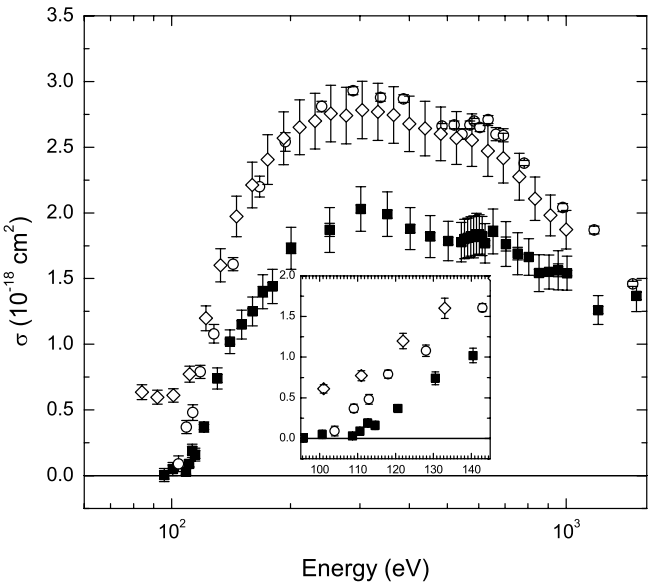

FIG. 10.—Experimental measurements for the absolute EII cross sections of O^{4+}. The solid squares represent the current experimental work, the open circles are the data of Falk et al. (1983) and the open diamond symbols are the data of Loch et al. (2003).

of approximately 5–24 eV. The bottom panel of Figure 9 gives the ratio of our CADW results and the data of Bell et al. (1983), Arnaud & Rothenflug (1985), and Dere (2007) to the recommended ground state RMPS rate coefficient.

As for the C^{2+} ratios, the Arnaud & Rothenflug data closely follow that of the CADW, which range from 5%–10% higher than the ground state RMPS rate coefficients in the CIE region. The data of Bell et al. are 10%–20% higher over this same region. The rate coefficients of Dere (2007) exhibit a good agreement with the ground state RMPS rate coefficients over the temperature range of the CIE region; being approximately 5%–10% larger. In the high electron temperature region, $k_B T_e > 100$ eV, the rate coefficient ratios of CADW and Arnaud & Rothenflug to the ground state RMPS are no more than approximately 4% higher while the Bell et al. and Dere data are approximately 15% higher.

We have scaled our pure ground and metastable RMPS rate coefficients according to equations (10) and (11) and fitted them using equation (12). The fit parameters are given in Table 6. For N^{3+} the error in our fits was less than 3% for the ground rate coefficients and less than 4% for the metastable rate coefficients. For much of the temperature range, the error was less than 2%. Our recommended RMPS rate coefficients are also tabulated in Table 7.

5.3. $O^{4+} \rightarrow O^{5+}$

Our experimental O^{4+} EII cross section data and uncertainties are given in Table 4. Figure 10 shows the present measurements of the O^{4+} EII cross sections, with a metastable fraction of 0.24 ± 0.07, compared with the measurements of Falk et al. (1983) and Loch et al. (2003). Falk et al. estimate a metastable fraction of 0.90 in their ion beam, while Loch et al. do not explicitly state a metastable fraction estimation; however, they note the presence of a low-energy plateau in the measured EII cross sections below the metastable ionization potential of 103.6 eV. Given that they use an ECR ion source similar in operation to that used in this work, one would expect that they would have a metastable fraction more similar to this work rather than the 0.90 metastable fraction of Falk et al., which used a different type of ion source. This is partially supported by the comparisons of N^{3+} experimental data made in the previous section, where the Falk et al. data are consistently larger than the current measurements due to their higher metastable fraction. It is more likely that this plateau in the cross section could be a systematic linear offset and, if we assume this is the case, then the data of Loch et al. are within total absolute uncertainty of the current experimental data. These adjusted Loch et al. data are show in Figure 11, along with the current experimental results, as a comparison to the CADW and the RMPS theory results, assuming a 0.24 metastable fraction.

Excitation-autoionization contributions were calculated using the CADW method. For the O^{4+} ion, excitation of a $1s$ electron makes a small contribution to the ionization cross section for both the ground and metastable cross sections. For both the ground and metastable terms the $1s$ EA contribution starts near 550 eV. In this case, the $1s$ contribution to the total aligns with a small increase observed in the experimental cross section in this region. For the $2s2p\ ^3P$ metastable term, the first autoionizing configuration accessible via excitation of a $2s$ electron is the $1s^2 2p6s$ configuration.

The dashed curves in Figure 11 represent the mixed ground state and metastable term contributions at the metastable fraction measured using the gas attenuation technique. We note that the mixed ground and metastable RMPS results, at the measured metastable fraction of 0.24, tend to be higher than the experimental measurements over the lower energy range investigated. In the region near the peak of the cross section, we note that both the RMPS and the CADW results are slightly higher than the current experimental results with the CADW being highest. In the near-threshold region, the mixed RMPS and the mixed CADW results tend to agree with each other; however, they are both slightly higher than the observed experimental values. We have

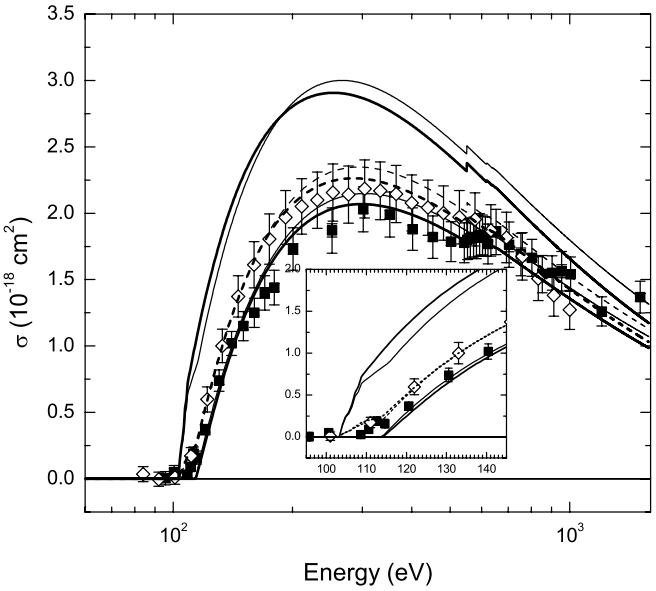

FIG. 11.—Current experimental measurements for O^{4+} (*filled squares*) are compared with CADW (*thin solid curves*) and RMPS (*thick solid curves*) theoretical cross sections for both ground state (*bottom solid curves*) and metastable term (*top solid curves*) ions. The dashed curves of each line type represent the admixture of ground state and metastable term cross sections at the experimentally inferred ion beam metastable fraction of 0.24. The adjusted (see text) experimental data of Loch et al. (2003, *open diamonds*) is also shown for comparison.

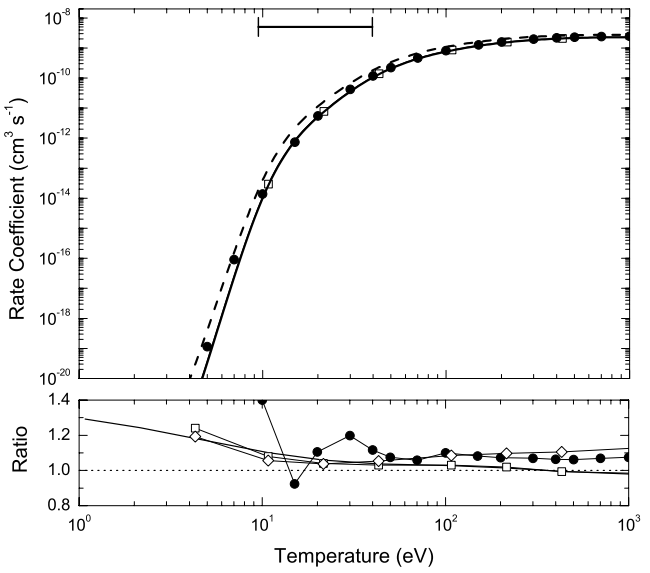

FIG. 12.—*Top*: Maxwellian rate coefficients for EII of O^{4+}. The thick solid curve represent the pure ground state RMPS results, the filled circles represent the rate coefficient recommended by Bell et al. (1983) and the open squares represent the rate coefficient recommended by Arnaud & Rothenflug (1985). The dashed curve represents the RMPS rate coefficient for the pure metastable $2s2p\ ^3P$ term. The temperature range for >1% fractional abundance in the CIE regime is shown by the horizontal line at the top of the plot (Bryans et al. 2006). The data of Dere (2007) are not plotted in the top panel for clarity. *Bottom*: Ratio relative to the ground state RMPS rate coefficient for our CADW results (*solid curve*), the Bell et al. (1983) data (*filled circles*), the Arnaud & Rothenflug (1985) data (*open squares*), and the Dere (2007) data (*open diamonds*). The lines interconnecting symbols are only meant to guide the eye.

also included, for comparison, the experimental results of Loch et al. (2003). These measurements should reflect a similar metastable fraction given that they used a similar type of ion source. It can be seen in Figure 11 that the Loch et al. data agree well with the mixed RMPS results over most of the energy range investigated and also strongly agree in the near threshold region. It should be noted, however, that while the Loch et al. data tend to exhibit a better agreement with the mixed theoretical results, the uncertainty of the measurements are within those of the current measurements and neither data set can be weighted more preferentially. This aspect points out the underlying caveat that theoretical results are often only as accurate as the experimental data to which they are benchmarked. The RMPS results represent our recommended EII cross sections. Our recommended cross sections can be reproduced using the Rost & Pattard (1997) fitting model parameters given in Table 5.

In comparing our recommended ground state RMPS cross section for O^{4+} to the distorted Coulomb-Born with exchange calculations of Jakubowicz & Moores (1981) we find that their results are approximately 8% larger than RMPS at the peak of the cross section.

We have generated our recommended Maxwellian rate coefficients using the pure ground and metastable RMPS cross section results. Figure 12 shows our recommended data, for both the ground state and metastable term, compared with rate coefficients archived in the literature. The range over which the fractional abundance of O^{4+} is greater than 1% in the CIE regime is given at the top of the figure (Bryans et al. 2006). This covers a temperature range of approximately 10–40 eV. The bottom panel of Figure 12 gives the ratio of our CADW results and the data of Bell et al. (1983), Arnaud & Rothenflug (1985), and Dere (2007) relative to our recommended ground state RMPS rate coefficient.

In the CIE zone, the ratios of the Arnaud & Rothenflug data, again, closely follow that of the CADW, which range from 3%–10% higher than the ground state RMPS rate coefficients. The data of Bell et al. average 12%–40% higher over this same region of fractional abundance. The data of Dere, in the CIE region, is approximately 5% higher than the RMPS rate coefficients, following that of Arnaud & Rothenflug and CADW. In the high electron temperature region, $k_B T_e > 100$ eV, our CADW and the Arnaud & Rothenflug rate coefficient ratios agree with the ground state RMPS rate coefficients, while the Bell et al. data are approximately 6%–10% higher than the RMPS rate coefficients. The rate coefficients of Dere tend to follow those of Bell at al. and are approximately 9%–17% higher than the RMPS rate coefficients.

We have scaled our pure ground and metastable RMPS rate coefficients according to equations (10) and (11) and fitted them using equation (12). The fit parameters are given in Table 6. For O^{4+} the error in our fit was less than 4% for both the ground and metastable rate coefficients, with the error being less than 3% for most of the temperature range. Our recommended RMPS rate coefficients are also tabulated in Table 7.

6. SUMMARY

We report on recent measurements of the electron-impact single ionization cross sections for Be-like C^{2+}, N^{3+}, and O^{4+} forming Li-like ions. We have independently measured the metastable fractions in the ion beams for each ion, inferring metastable fractions of 0.46, 0.30, and 0.24 for C^{2+}, N^{3+}, and O^{4+}, respectively. We compare our measured cross sections to CADW and RMPS theoretical results, and in all cases find that the RMPS results provide better overall agreement with the experimental measurements, and represent our recommended cross section data for each of these ions. We have generated ionization rate coefficients for the ground state and metastable term for each of the ions, using

the RMPS cross sections. The RMPS rate coefficients have been tabulated and scaled temperatures and rate coefficients have been fitted following the method by Dere (2007). Fit parameters have been provided to reproduce our recommended ground and metastable Maxwellian rate coefficients.

The authors thank J. M. Laming for stimulating discussions. This work was supported in part by the Office of Fusion Energy Sciences and the Office of Basic Energy Sciences of the U.S. Department of Energy under Contract DE-AC05-00OR22725 with UT-Battelle, LLC, and by NASA under Award NNH04AA151 issued through the Sun-Earth Connection Division's Solar and Heliospheric Physics Supporting Research and Technology Program. and under Award NNH04AA72I issued through the Astronomy and Physics Research and Analysis Program. M. F. and E. M. B. were appointed via the ORNL Postdoctoral Research Associates Program administered jointly by the Oak Ridge Institute for Science and Education and Oak Ridge National Laboratory. R. D. T. acknowledges the support of the Swedish Research Council (VR). C. B. P., S. D. L., and M. S. P. gratefully acknowledge the support from a grant by the U.S. Department of Energy DE-FG02-05ER54819. P. B., W. M., and D. W. S. were supported in part by the NASA Solar and Heliospheric Physics Supporting Research and Technology Program and the NASA Astronomy and Astrophysics Research and Analysis Program.

REFERENCES

Arnaud, M., & Raymond, J. 1992, ApJ, 398, 394
Arnaud, M., & Rothenflug, R. 1985, A&AS, 60, 425
Badnell, N. R. 1997, J. Phys. B, 30, 1
Ballance, C. P., & Griffin, D. C. 2004, J. Phys. B, 37, 2943
Bannister, M. E. 1996, Phys. Rev. A, 54, 1435
Bartschat, K. 1998, Comput. Phys. Commun., 114, 168
Bell, K. L., Gilbody, H. B., Hughes, J. G., Kingston, A. E., & Smith, F. J. 1983, J. Phys. Chem. Ref. Data, 12, 891
Berengut, J. C., Loch, S. D., Balnance, C. P., & Pindzola, M. S. 2007, J. Phys. B, 40, 1331
Bliek, F. W., Hoestra, R., Bannister, M. E., & Havener, C. C. 1997, Phys. Rev. A, 56, 426
Brazuk, A., Dijkkamp, D., Drentje, A. G., de Heer, F. J., & Winter, H. 1984, J. Phys. B, 17, 2489
Bryans, P., Badnell, N. R., Gorczyca, T. W., Laming, J. M., Mitthumsiri, W., & Savin, D. W. 2006, ApJS, 167, 343
Burgess, A., & Tully, J. A. 1992, A&A, 254, 436
Colgan, J., Loch, S. D., Pindzola, M. S., Ballance, C. P., & Griffin, D. C. 2003, Phys. Rev. A, 68, 032712
Cowan, R. D. 1981, The Theory of Atomic Structure and Spectra (Berkeley: Univ. California)
Dere, K. P. 2007, A&A, 466, 771
Doerfert, J., Träbert, E., Wolf, A., Schwalm, D., & Uwira, O. 1997, Phys. Rev. Lett., 78, 4355
Falk, R. A., Stefani, G., Camilloni, R., Dunn, G. H., Phaneuf, R. A., Gregory, D. C., & Crandall, D. H. 1983, Phys. Rev. A, 28, 91
Fogle, M., Badnell, N. R., Glans, P., Madzunkov, S., Abdel-Naby, Sh. A., Pindzola, M. S., & Schuch, R. 2005, A&A, 442, 757
Ganas, P. S., & Green, A. E. S. 1981, J. Quant. Spectrosc. Radiat. Transf., 25, 265
Gardner, L. D., Bayfield, J. E., Koch, P. M., Sellin, I. A., Pegg, D. J., Peterson, R. S., Mallory, M. L., & Crandall, D. H. 1979, Phys. Rev. A, 20, 766
Geller, R. 1996, Electron Cyclotron Resonance Ion Sources and ECR Plasmas (London: Institute of Physics)
Ghavamian, P., Laming, J. M., & Rakowswki, C. E. 2007, ApJ, 654, L69
Glass, R. 1982, Ap&SS, 87, 41
Gregory, D. C., Dittner, P. F., & Crandall, D. H. 1983, Phys. Rev. A, 27, 724
Griffin, D. C., et al. 2005, J. Phys. B, 38, L199
Gu, M. F. 2002, ApJ, 579, L103
Hamdan, M., Birkinshaw, K., & Hasted, J. B. 1978, J. Phys. B, 11, 331
Ishii, K., Itoh, A., & Okuno, K. 2004, Phys. Rev. A, 70, 042716
Jakubowicz, H., & Moores, D. L. 1981, J. Phys. B, 14, 3733
Kato, T., Masai, K., & Arnaud, M. 1991, NIFS-DATA-14 (Nagoya: National Institute for Fusion Science)
Laming, J. M., Raymond, J. C., McLaughlin, B. M., & Blair, W. P. 1996, ApJ, 472, 267
Laughlin, C. 1980, Phys. Lett. A, 75, 199
Lennon, M. A., Bell, K. L., Gilbody, H. B., Hughes, J. G., Kingston, A. E., Murray, M. J., & Smith, F. J. 1988, J. Phys. Chem. Ref. Data, 17, 1285
Loch, S. D., Colgan, J., Pindzola, M. S., Westermann, M., Scheuermann, F., Aichele, K., Hathiramani, D., & Salzborn, E. 2003, Phys. Rev. A, 67, 042714
Loch, S. D., Ludlow, J. A., Pindzola, M. S., Whiteford, A. D., & Griffin, D. C. 2005b, Phys. Rev. A, 72, 052716
Loch, S. D., Pindzola, M. S., Ballance, C. P., Griffin, D. C., Badnell, N. R., O'Mullane, M. G., Summers, H. P., & Whiteford, A. D. 2002, Phys. Rev. A, 66, 052708
Loch, S. D., et al. 2005a, Phys. Rev. A, 71, 012716
Mazzotta, P., Mazzitelli, G., Colafrancenso, S., & Vittorio, N. 1998, A&AS, 133, 403
McCarthy, I. E., & Stelbovics, A. T. 1983, Phys. Rev. A, 28, 1322
McGuire, E. J. 1997, J. Phys. B, 30, 1563
Meyer, F. W. 2001, in Trapping Highly Charged Ions: Fundamentals and Applications, ed. J. Gillaspy (New York: Nova Science), 117
Mitnik, D. M., Griffin, D. C., Ballance, C. P., & Badnell, N. R. 2003, J. Phys. B, 36, 717
Mitnik, D. M., Pindzola, M. S., Griffin, D. C., & Badnell, N. R. 1999, J. Phys. B, 32, L479
Moores, D. L. 1978, J. Phys. B, 11, L403
NIST. 2007, NIST Atomic Spectra Database ver. 3.1.2, http://www.physics.nist.gov/PhysRefData/ASD/index.html
Peart, B., Walton, D. S., & Dolder, K. T. 1969, J. Phys. B, 2, 1347
Phaneuf, R. A., Janev, R. K., & Pindzola, M. S. 1985, ORNL-6090, Atomic Data for Fusion, Vol. 5: Collisions of Carbon and Oxygen Ions with Electrons, H, H2 and He (Oak Ridge: ORNL)
Pindzola, M. S., Griffin, D. C., Badnell, N. R., & Summers, H. P. 1996, Nucl. Fusion Suppl., 6, 117
Pindzola, M. S., Griffin, D. C., & Bottcher, C. 1986, in Atomic Processes in Electron-Ion and Ion-Ion Collisions, Vol. 145 of NATO Advanced Studies Institute, Ser. B: Physics, ed. F. Brouillard (New York: Plenum), 75
Pindzola, M. S., Griffin, D. C., Bottcher, C., Younger, S. M., & Hunter, H. T. 1987, Nucl. Fusion Special Suppl., 1, 21
Pindzola, M. S., Griffin, D. C., Buie, M. J., & Gregory, D. C. 1991, Phys. Scr., T37, 35
Pindzola, M. S., Mitnik, D. M., Colgan, J., & Griffin, D. C. 2000, Phys. Rev. A, 61, 052712
Rost, J. M., & Pattard, T. 1997, Phys. Rev. A, 55, R5
Salop, A. 1976, Phys. Rev. A, 14, 2095
Sampson, D. H. 1986, Phys. Rev. A, 34, 986
Savin, D. W. 2005, in X-Ray Diagnostics of Astrophysical Plasmas: Theory, Experiment, and Observation, ed. R. K. Smith (Melville: AIP), 297
Schmieder, R. W. 1973, Phys. Rev. A, 7, 1458
Tawara, H. 1992, NIFS-DATA-17, Electron Stripping Cross Sections for Light Impurity Ions in Colliding with Atomic Hydrogens Relevant to Fusion Research (Nagoya: National Institute for Fusion Science)
Träbert, E., Wolf, A., & Gwinner, G. 2002, Phys. Lett. A, 295, 44
Turner, B. R., Rutherford, J. A., & Compton, D. M. J. 1968, J. Chem. Phys., 48, 1602
Unterreiter, E., Schweinzer, J., & Winter, H. 1991, J. Phys. B, 24, 1003
Voronov, G. S. 1997, At. Data Nucl. Data Tables, 65, 1
Vujović, M., Matić, M., Čobić, B., & Gordeev, Yu S. 1972, J. Phys. B, 5, 2085
Wannier, G. H. 1953, Phys. Rev., 90, 817
Woodruff, P. R., Hublet, M.-C., Harrison, M. F. A., & Brook, E. 1978, J. Phys. B, 11, L679
Yamada, I., et al. 1989, J. Phys. Soc. Japan, 58, 1585
Younger, S. M. 1981a, Phys. Rev. A, 24, 1272
———. 1981b, Phys. Rev. A, 24, 1278